Intelligent Pharmacy 4 (2026) 126–138

Contents lists available at ScienceDirect

Intelligent Pharmacy

journal homepage: www.keaipublishing.com/en/journals/intelligent-pharmacy

Full length article

Diabetes-associated metabolic-immune signature stratifies survival and immunotherapy response in pancreatic adenocarcinoma through multi-omics integration

Le Tang[a,c], Mengwei Yang[a,c], Tongji Xie[a,c], Guangyu Fan[a], Haohua Zhu[a], Jiari Yao[a], Xiaohong Han[b,*], Yuankai Shi[a,**]

[a] Department of Medical Oncology, Beijing Key Laboratory of Key Technologies for Early Clinical Trial Evaluation of Innovative Drugs for Major Diseases, National Cancer Center/National Clinical Research Center for Cancer/Cancer Hospital, Chinese Academy of Medical Sciences & Peking Union Medical College, Beijing, China
[b] Clinical Pharmacology Research Center, Peking Union Medical College Hospital, State Key Laboratory of Complex Severe and Rare Diseases, NMPA Key Laboratory for Clinical Research and Evaluation of Drug, Beijing Key Laboratory of Key Technologies for Early Clinical Trial Evaluation of Innovative Drugs for Major Diseases, Chinese Academy of Medical Sciences & Peking Union Medical College, Beijing, China

ARTICLE INFO

Keywords:
Pancreatic adenocarcinoma
Diabetes mellitus
Prognostic model
Tumor immune microenvironment
Single cell
Spatial transcriptomics

ABSTRACT

Objective: Pancreatic adenocarcinoma (PAAD) poses a significant threat, especially to patients with diabetes mellitus (DM). While numerous studies have explored prognostic factors for pancreatic cancer, research specifically focusing on PAAD patients with DM remains scarce. This study aims to address this gap by identifying differentially expressed genes (DEGs) between DM and non-DM individuals and developing a reliable prognostic model to predict overall survival (OS) in PAAD patients with DM.

Methods: PAAD patients with DM were divided into a training group (70%) and a test group (30%). Univariate COX analysis was used to screen genes associated with OS. A 10-gene risk model (*ACACA*, *ATG7*, *DEFB123*, *FSTL3*, *NIPSNAP3B*, *RASSF1*, *RBPJ*, *SLC35F2*, *SLC37A1* and *ZC3H12D*) was constructed via LASSO-penalized COX regression combined with ten-fold cross-validation. Additionally, multi-omics findings were integrated, and in vitro functional studies were conducted to validate the oncogenic roles of key metabolic regulators (*ACACA* and *ATG7*) under high-glucose conditions.

Results: The constructed model demonstrated strong predictive ability, with a *C-index* of 0.83 in the training group and 0.76 in the test group, indicating good performance across both cohorts. Further analysis revealed that the high-risk group exhibited a tumor-growth and angiogenic phenotype (which may drive rapid tumor progression), while the low-risk group showed an immune-active phenotype (suggesting a favorable immunological microenvironment).

Conclusions: This prognostic model can predict the OS of PAAD patients with DM. Low-risk patients may be suitable candidates for immunotherapy, whereas high-risk patients may benefit from alternative strategies such as anti-angiogenic therapy.

1. Introduction

Pancreatic adenocarcinoma (PAAD) stands as a highly lethal disease, bearing an exceptionally grim prognosis. It ranks as the third leading cause of cancer-related mortality.[1] The prevalence of diabetes mellitus (DM) in PAAD is notably high.[2] Up to 40%–65% of PAAD patients have DM or pre-DM at diagnosis, and about 25% have new-onset DM.[3,4] The onset of DM represents a critical risk factor, as individuals with DM face a 3.05-fold heightened risk of developing PAAD. Additionally, for every 0.56 mmol/L increase in fasting blood glucose levels, there is a corresponding 14% escalation in the likelihood of PAAD occurrence.[5–8] While studies have delved into markers or prognostic models impacting the prognosis of

* Corresponding author.
** Corresponding author.
E-mail addresses: mynameismary@yeah.net (L. Tang), xy279324@163.com (M. Yang), 1300159525@qq.com (T. Xie), fgypumc@163.com (G. Fan), zhuhaohua2020@qq.com (H. Zhu), carrieyao531@163.com (J. Yao), hanxiaohong@pumch.cn (X. Han), syuankai@cicams.ac.cn (Y. Shi).
Peer review under the responsibility of Editorial Board of Intelligent Pharmacy.
[c] Le Tang, Mengwei Yang and Tongji Xie contributed equally to this article as co-first authors.

https://doi.org/10.1016/j.ipha.2025.12.004
Received 19 November 2025; Received in revised form 16 December 2025; Accepted 16 December 2025
Available online 18 December 2025
2949-866X/© 2026 The Authors. Publishing services by Elsevier B.V. on behalf of Higher Education Press and KeAi Communications Co. Ltd. This is an open access article under the CC BY license (http://creativecommons.org/licenses/by/4.0/).

PAAD patients, a critical gap persists: there is a notable lack of prognostic models specifically designed for PAAD patients with comorbid DM that not only predict survival but also stratify patients for differential therapeutic interventions based on underlying metabolic-immune signatures.[9–12] Moreover, the functional roles of DM-associated genes in shaping the aggressive phenotype of PAAD under hyperglycemic conditions remain underexplored. This study aimed to explore the gene expression characteristics of PAAD patients by integrating analyses of bulk, single-cell and spatial transcriptional profiling. Additionally, we sought to develop a prognostic model based on DM status to aid in the clinical management of PAAD patients, particularly those with DM.

2. Method

2.1. Data acquisition and processing

Bulk, single-cell and spatial transcriptional data, along with clinical characteristics of patients with PAAD, were downloaded from the Genomic Data Commons Data Portal of The Cancer Genome Atlas (TCGA) (portal.gdc.cancer.gov) and the GEO database (www.ncbi.nlm.nih.gov/geo). To assess the prognostic potential of the DM-based signature, we extracted bulk transcriptomics data along with clinical information from TCGA and GSE79670 datasets.[13] For both TCGA-PAAD and GSE79670, we included primary tumor samples with available gene expression profiles, overall survival (OS) and DM status. Samples lacking any of these clinical annotations were excluded from the analysis, and duplicate samples, if any, were removed. The "sva" package (www.bioconductor.org.) was used to remove batch effects of transcriptional data of TCGA and GSE79670 in order to train and test a DM-based PAAD prognostic model. Furthermore, immunotherapy data from GSE179351[14] cohort were acquired to explore the utility of the prognostic model in predicting the efficacy of immunotherapy. In addition, single-cell RNAseq (scRNA-seq) data of PAAD tissue samples from GSE154778[15] and spatial transcriptomics data of GSE224411[16] were utilized for further validation of the prognostic model and to elucidate the molecular mechanisms underlying differences in prognosis.

2.2. Construction and validation of DM-based PAAD prognostic model

The differentially expressed genes (DEGs) between PAAD patients with and without DM were performed using the Wilcoxon rank-sum test. Subsequently, p value was adjusted for multiple testing using the false discovery rate (*FDR*) method. Genes with a raw $p < 0.05$ and $FDR < 0.25$ were selected as DEGs. PAAD patients with DM were randomly divided into a training cohort comprising 70% of the patients and a test cohort consisting of the remaining 30%. Subsequently, univariate COX regression analysis was conducted to identify OS-associated genes from the pool of DEGs with a $p < 0.05$ in the training cohort. The least absolute shrinkage and selection operator (LASSO)-penalized COX regression and ten-fold cross validation were employed for model training and model selection, respectively. The risk score, derived from the expression and coefficient of each gene, was calculated, and its efficacy was verified in both training and test cohort. The median risk score was utilized as the cut-off value to stratify PAAD patients with DM into high and low risk groups.

2.3. Pathway enrichment analysis

Gene Set Variation Analysis (GSVA) and STRING were employed to assess the relative activity of signaling pathways and biological processes. This was accomplished using the "GSVA" and "GSEABase" packages, along with the STRING resource available online at string-dp.org/.[17–19]

Information on gene sets within the "HALLMARK", "Kyoto Encyclopedia of Genes and Genomes (KEGG)", and "Gene Ontology (GO)" categories was acquired from www.gsea-msigdb.org/gsea/msigdb/index.jsp. For the GSVA results, we conducted the Wilcoxon rank-sum test between the high-risk group and the low-risk group. Subsequently, we calculated the difference in median GSVA scores (ΔmGS) between these groups to illustrate the trend of activity for each signaling pathway and biological process. We presented the ΔmGS values for a total of 1350 signaling pathways and biological processes, encompassing various categories such as metabolism and energy, extracellular matrix (ECM) and metastasis, genetic and epigenetic information, immunity, cell cycle, and cell death. These results were depicted using radar plots, Nightingale rose diagrams, and dumbbell plots.

2.4. Tumor immune microenvironment (TIME) analysis

The stromal and immune scores in tumor tissue were computed using the ESTIMATE method, facilitated by the "estimate" package.[20] CIBERSORT (cibersort.stanford.edu)[21] was conducted to determine the proportion of 22 distinct types of immune cells. For those sample with a $p < 0.05$ in the result of CIBERSORT, we used zero as the infiltration fraction of these immune cells. Single-sample Gene Set Enrichment Analysis (ssGSEA) was utilized to assess the scores of 28 different immune cell types using the "GSVA" package.[22]

2.5. Immune checkpoint inhibitors (ICIs)' effect analysis

Immunophenoscore (IPS) of TCGA cohort was acquired from The Cancer Immunome Atlas (TCIA) (tcia.at/home).[23,24] In order to validate the ICIs therapy expectations of PAAD patients with DM, we queried and extracted the real ICIs therapy data (GSE179351) from GEO database which was a single-arm, non-randomized, phase II trial (NCT03104439, 2017-05-10, Massachusetts General Hospital) combining radiation, ipilimumab and nivolumab in patients with metastatic microsatellite-stable colorectal cancer ($N = 40$) and PAAD ($N = 25$) with an ECOG performance status of 0 or 1. We obtained clinical data for 10 PAAD patients which included RNA sequencing data in the PAAD cohort. Among these patients, the median OS was 5.53 months, and the median progression-free survival (PFS) was 2.68 months. Among them, one patient exhibited stable disease (SD), one partial response (PR) and one complete response (CR), while seven patients showed disease progression (PD). Notably, the patient diagnosed with PAAD presented with widely metastatic disease at the time of diagnosis.

2.6. Dimension reduction and clustering analysis of single-cell transcriptional data

The single-cell transcriptional data of GSE154778 was obtained. Cells that exhibited a minimum of 600 detected genes and a mitochondrial percentage below 15% were retained for analysis. Subsequently, the data underwent normalization to transcript copies per 10,000 and log-normalization to mitigate sequencing depth variability. The top 2000 most variable genes were identified using the FindVariableFeatures function and subsequently utilized for principal component analysis (PCA). To mitigate batch effects within the datasets, we applied the Harmony algorithm from the "Harmony" package before conducting the clustering analysis. Cell subtypes were then determined using the FindNeighbors and FindCluster functions. We employed curated markers to annotate cells as follows: epithelial cells (EPCAM, KRT8, KRT18), fibroblasts (COL1A1, COL1A2, DCN), endothelial cells (CLDN5, VWF, PECAM1), T cells (CD2, CD3D, CD3E, CD3G), B cells (CD79A, CD79B), myeloid cells (CD14, CD16, CD68).

2.7. The construction of risk score in single-cell data

We proceeded to score individual cells for risk using the "AUCell" package. Initially, for each cell, we computed gene expression rankings within the expression matrix using the AUCell_buildRankings function, with default parameters. Subsequently, for each gene set and cell, we

calculated the area under the curve (AUC) using the AUCell_calcAUC function, based on gene expression rankings. The AUC values represent the fraction of genes within the top-ranking genes for each cell that are defined as part of the pathway gene set.

2.8. Differential expression analysis and gene set enrichment analysis (GSEA) in single-cell data

We employed the FindMarkers function in the "Seurat" package, utilizing the MAST differential expression analysis method, to identify the DEGs. This analysis was conducted with a log_2FC cut-off of 0.25 and only.pos set to False. Additionally, we utilized GSEA in the "fgsea" package to assess the enrichment of "HALLMARK" gene sets, as well as Biological Process gene sets from GO and KEGG.

2.9. Clustering analysis of spatial transcriptomics

Spatial transcriptomics data underwent clustering analysis using "Seurat". Spots with fewer than 500 detected genes or more than 6000 genes, and those with over 20% mitochondrial counts, were filtered out. Gene expression was adjusted using Seurat's SCT normalization algorithm. PCA-based dimension reduction was performed, extracting the first 20 principal components for Louvain clustering to define cell types at a resolution of 0.8. UMAP (Uniform Manifold Approximation and Projection) is a dimension reduction technique used to visualize high-dimensional data in a lower-dimensional space, typically two or three dimensions. UMAP was used for visualizing high-dimensional data in two or three dimensions.

2.10. Cells and cell culture

Human PAAD cell lines MIA PaCa-2 (CL-0627) and PANC-1 (CL-0184) were obtained from Procell (Wuhan, China). Cell line authentication was confirmed via short tandem repeat profiling. Cells were cultured in DMEM/HIGH GLUCOSE medium (Cytiva, Shanghai, China), supplemented with 10% fetal bovine serum (FBS) (Gibco, USA) and 1% penicillin - streptomycin. Cultures were incubated at 37 °C in a humidified incubator containing 5% CO_2. To model different glucose environments, cells were treated with isotonic media containing physiological normoglycemia (5.5 mM), high glucose (25 mM) or severe hyperglycemic (50 mM) concentrations.

2.11. Cell transfection

Specific siRNAs targeting *ACACA* and *ATG7* were synthesized and purchased from DDXCELL (Shanghai, China). Cells transfected with siRNAs were compared to the corresponding negative control. Lipofectamine™ 3000 (Thermo Fisher Scientific, USA) and Opti-MEM (Gibco, USA) were used as transfection reagent and medium. 24 hours (h) after siRNA transfection, total RNA was extracted and knockdown efficiency was initially assessed by quantitative reverse transcription polymerase chain reaction (qRT-PCR). Samples showing a clear reduction (>70%) in *ACACA* or *ATG7* mRNA levels were selected for further analysis. 48 h after transfection, protein lysates were collected for western blot to verify the decrease in ACACA or ATG7 protein expression. Cells were used for subsequent experiments 48 h post-transfection.

2.12. Cell migration assay

Cell migration was evaluated using transwell chambers (Corning, USA). The lower chamber was filled with 600 ul medium supplemented with 10% FBS, while the upper chamber contained 200 ul serum-free cell suspension at a density of 5×10^5 cells/ml. After 24 h of incubation at 37 °C with 5% CO_2, non-migratory cells on the upper surface were removed using a cotton swab. Migrated cells on the lower surface were fixed with 4% paraformaldehyde in PBS and stained with 0.1% crystal violet solution. Images were acquired after air-drying the chambers.

2.13. Cell cycle assay

Cells were fixed with 70% ethanol and stained using the Cell Cycle Assay Kit - PI/RNase Staining (Dojindo laboratories, Japan) according to the manufacturer's instructions. A total of 1,000,000 cells per sample were analyzed by flow cytometry.

2.14. Cell apoptosis assay

Apoptotic and viable cells were assessed using the Annexin V-FITC Apoptosis Detection Kit (Dojindo laboratories, Japan) following the operating instruction. A total of 10,000 cells per sample were analyzed by flow cytometry.

2.15. Proliferation assay

48 h after transfection, cells were harvested and seeded into 96-well plates (Corning, USA) at a density of 2×10^3 cells pre well, incubated in at 37 °C with 5% CO_2. After 12 h of attachment, cell viability was assessed at 0, 24, 48 and 72 h using the Cell Counting Kit (CCK)-8 assay (Dojindo laboratories, Japan). OD values at 450 nm were measured and used to determine cell viability.

2.16. Statistical analysis

For our statistical analyses, we utilized R 4.2.3. We applied the Wilcoxon rank-sum test for continuous and rank variables, and performed the Fisher exact test and Pearson chi-square test for unordered categorical variables. Correlational analyses were conducted using Spearman analysis, and the results were visualized in scatter plot, chord plot, or forest plot formats. For survival analysis, Cox proportional hazards regression analysis and the log-rank test were conducted using the "survival" and "survminer" packages. Statistical significance was determined with a threshold of $p < 0.05$ and $FDR < 0.25$, both considered simultaneously.

3. Results

3.1. Data acquisition and processing

A detailed flowchart of this study was presented in Fig. 1. 197 PAAD patients (Table-1) with both bulk transcriptional data and OS information were enrolled. There were 585 DEGs (Supplementary Table-1, Fig. S1a) between PAAD patients with and without DM. The pathway enrichment results of these DEGs were shown in Fig.S1b and Fig.S1c. The up-regulated pathways contain many immune-related pathways, including "GO:0050870: Positive regulation of T cell activation" and "GO:0001771: Immunological synapse formation". Whereas the down-regulated pathways were related to cell connection, including "GO:0045296: Cadherin binding", "GO:0005912: Adherens junction" and "GO:0030054: Cell junction)". Other pathway enrichment results of the 585 DEGs were listed in Supplementary Table-2.

3.2. Construction of DM-based PAAD prognostic model

Among 60 PAAD patients with DM, 42 were split into the training cohort and 18 into the test cohort, and the relationship between 585 DM-related DEGs with OS was investigated in the training cohort. Twenty-three OS-related DM-related DEGs (Supplementary Table-3) were screened as the input for LASSO-COX regression (Fig. S2a) and ten-fold cross validation (Fig. S2b), and a 10-gene model was built with the minimum partial likelihood deviance (at the $\lambda = 0.1004$). The risk score predictor was defined as: $0.434 \times ACACA + 0.119 \times ATG7 + 0.373 \times DEFB123 + 0.135 \times FSTL3 - 0.168 \times NIPSNAP3B -$

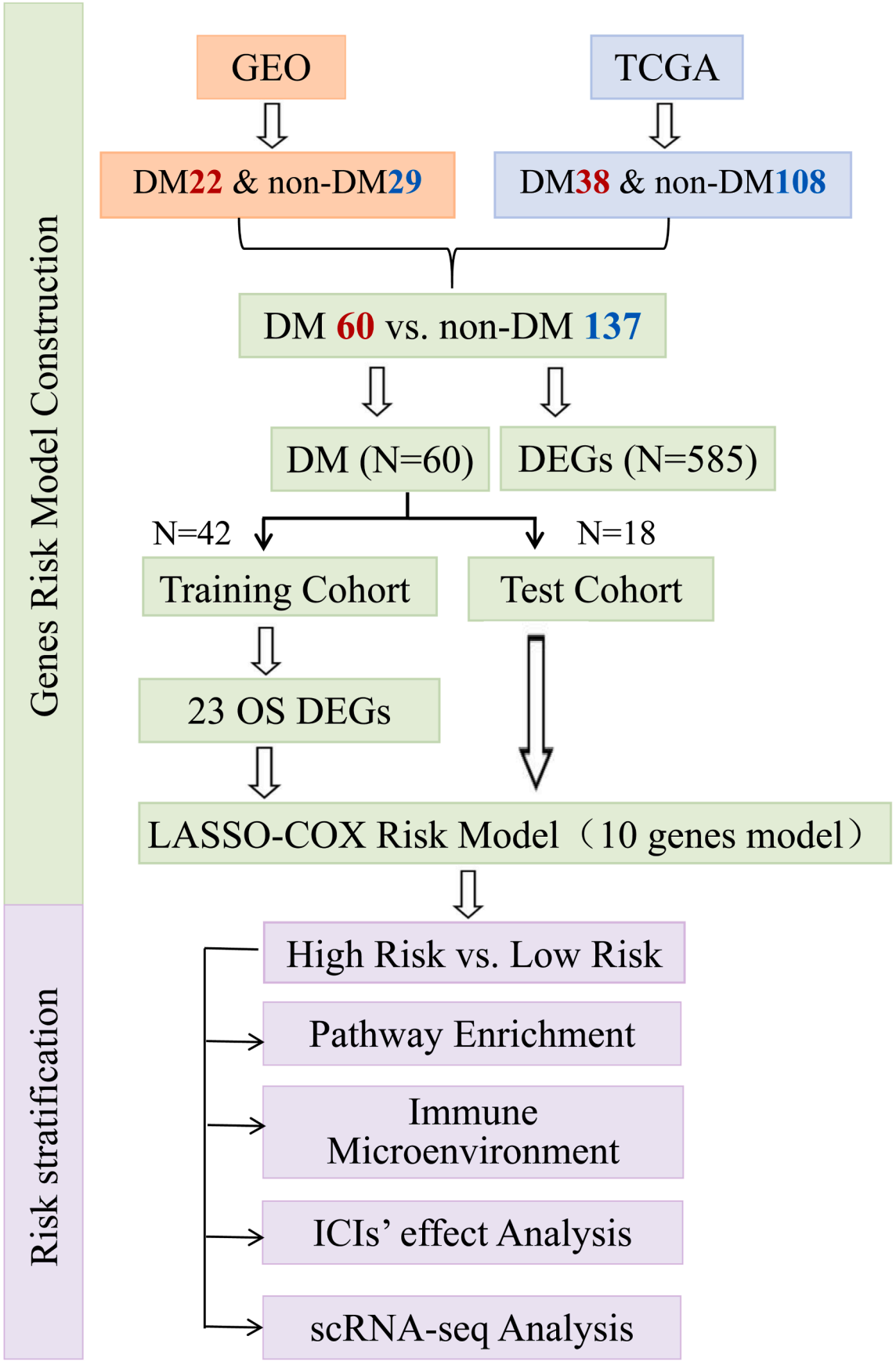


Fig. 1. Flowchart depicting the process of this multi-omics analysis.

Table 1
Clinical characteristics of PAAD with DM.

	Diabetes N = 60			Non-Diabetes N = 137	
	Group	Number	Proportion (%)	Number	Proportion (%)
Age	> 60	44	73.33	85	62.04
	< 60	16	26.67	52	37.96
Gender	male	39	65.00	73	53.29
	female	21	35.00	64	46.72
Stage-T	T3-T4	45	75.00	108	78.83
	T1-T2	14	23.33	28	20.44
	TX	1	1.67	1	0.73

0.069 × *RASSF1* + 0.225 × *RBPJ* + 0.364 × *SLC35F2* - 0.168 × *SLC37A1* - 0.145 × *ZC3H12D*. Then, the value of this risk model in predicting OS was calculated in both training and test cohorts. In the training cohort, the *C-index* of the model risk score (*C-index* = 0.83, hazard ratio [*HR*] = 7.61, 95% confidence interval [*CI*] 3.56–16.27, $p < 0.001$) was higher than that of all 10 genes in this model (Fig. 2a). In the test cohort, the *C-index* of the model risk score (*C-index* = 0.76, *HR* = 3.22, 95% *CI* 1.26–8.23, $p = 0.015$) is also relatively high among 585 DM-related DEGs (Fig. 2b). The correlation results between the model risk score and 10 genes in this model were showed in chord plot format (Fig.S2c & Fig.S2d). Uni/multivariate COX regression were performed to validate

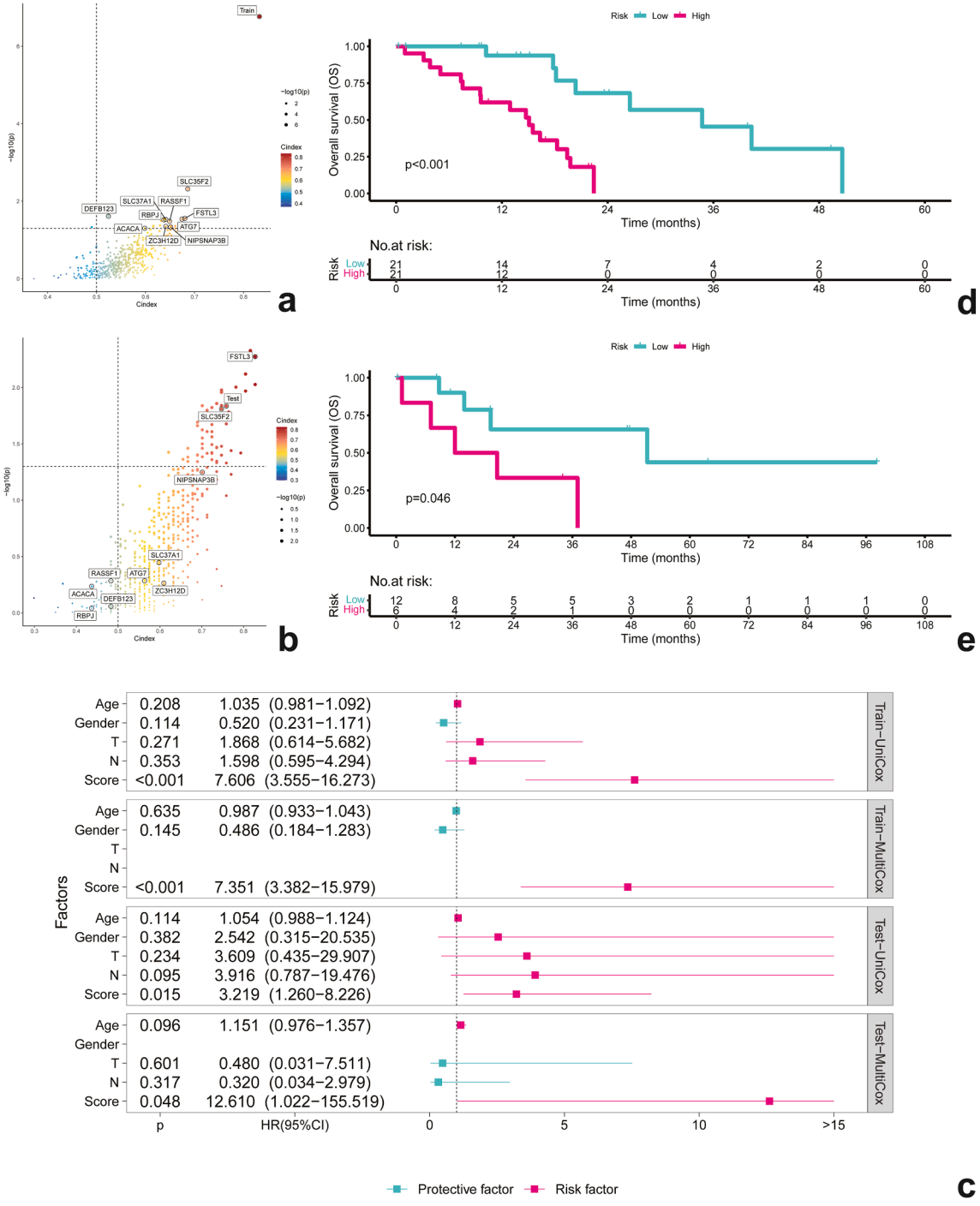


Fig. 2. The risk model to predict the OS for PAAD patients with DM. **(a)** Scatter plot for OS result of 585 DEGs in the Training cohort. **(b)** Scatter plot for OS result of 585 DEGs in the Test cohort. **(c)** Forest plot for the univariate and multivariate COX analysis. **(d)** KM curve for the Training cohort. **(e)** KM curve for the Test cohort.

the independently predictive value of the model risk score (Fig. 2c). In the univariate COX analysis, risk score of the model was a prognostic risk factor for OS in both the training cohort (*HR* = 7.61, 95% *CI* 3.56–16.27, $p < 0.001$) and test cohort (*HR* = 3.22, 95% *CI* 1.26–8.23, $p = 0.015$). Age and gender in the univariate COX result of training cohort as well as age, T stage and N stage in the univariate COX result of test cohort, were considered as potential influential factors of OS (with a $p < 0.25$) and enrolled into multivariate COX analysis of training and test cohort, respectively. The multivariate COX analysis showed that the model risk score was an independent prognostic risk factor for OS in PAAD patients with DM from both training (*HR* = 7.35, 95% *CI* 3.38–15.98, $p < 0.001$) and test (*HR* = 12.6, 95% *CI* 1.02–155.52, $p = 0.048$) cohorts.

To streamline the application of the DM-based risk model, we selected the median value of the model risk score (−0.054) as the cut-off point. Subsequently, PAAD patients with DM were stratified into two groups: high-risk and low-risk (Fig.S3a & Fig.S3b Supplementary Table-4). Furthermore, Kaplan–Meier analysis conducted on both the training (Fig. 2d) and test (Fig. 2e) cohorts revealed that patients categorized in the high-risk group exhibited a notably shorter median OS compared to those in the low-risk group.

3.3. Pathway enrichment analysis

To delve into the potential mechanism underlying the predictive efficacy of the DM-based risk model, we further performed GSVA. A total of 1350 genesets (Supplementary Table-5) associated tumor and its microenvironment were analyzed as a point of importance. The 1350 genesets were summarized into six classes by us according to the information of these genesets provided on the molecular signatures database (MSigDB), including 421 “Immunity”, 127 “Cell cycle”, 315 “Metabolism & energy”, 286 “Genetic and epigenetic information”, 129 “ECM & metastasis” and 72 “Cell death” genesets. There were 10.2% (43/421) “Immunity”, 90.6% (115/127) “Cell cycle”, 56.8% (179/315) “Metabolism & energy”, 58.7% (168/286) “Genetic and epigenetic information”, 67.4% (87/129) “ECM & metastasis” and 70.8% (51/72) “Cell death” genesets showed higher GSVA score in the high risk group (ΔmGS >0), whereas 89.8% (378/421) “Immunity”, 9.4% (12/127) “Cell cycle”, 43.2% (136/315) “Metabolism & energy”, 41.3% (118/286) “Genetic and epigenetic information”, 32.6% (42/129) “ECM & metastasis” and 29.2% (21/72) “Cell death” genesets showed higher GSVA score in the low risk group (ΔmGS <0) (Fig. 3a). Among the statistically significant gene sets identified, only 422 were retained after selection. Notably, 44.1% (56/127) of the “Cell cycle” gene sets were enriched in the high-risk group with statistical significance (ΔmGS >0, $p < 0.05$, and *FDR* < 0.25), while 53.4% (225/421) of the “Immunity” gene sets exhibited enrichment in the low-risk group with statistical significance (ΔmGS < 0, $p < 0.05$, and *FDR* < 0.25) (refer to Fig. 3b).

Consequently, we focused our further investigation on the “Cell cycle” and “Immunity” gene sets. Specifically, the “Immunity” gene sets were subdivided into seven subclasses: antigen processing-related (“Antigen”), B lymphocyte-related (“B_CELL”), cytokine-related (“Cytokine”), macrophage-related (“Macrophage”), natural killer-related (“NK”), T lymphocyte-related (“T_CELL”), and other immune-related (“Immune”) gene sets. Among the “Cell cycle” gene set and the seven subclasses of “Immunity” genesets, it was observed that “Cell cycle” had the highest number of statistically significant results in the high-risk group (56 gene sets, see Fig. S4a). Conversely, in the low-risk group, “T_CELL” exhibited the highest number of statistically significant results apart from the general “Immune” category (52 gene sets, see Fig. S4b).

As a result, we focused on the “Cell cycle” and “T_CELL” genesets with statistical significance and a relative strict criterion of *FDR* < 0.05 was used in the next step of research. Under this criterion, we screened a total of 24 “Cell cycle” and “T_CELL” genesets (Fig. 3c). All four “T_CELL” genesets exhibited a higher median GSVA score in the low-risk group. Conversely, nearly all 20 ″Cell cycle” genesets demonstrated a higher median GSVA score in the high-risk group. Notably, the geneset “GOBP_G1_TO_G0_TRANSITION” within the “Cell cycle” category displayed a higher median GSVA score in the low-risk group.

To understand the correlation between the model risk score and

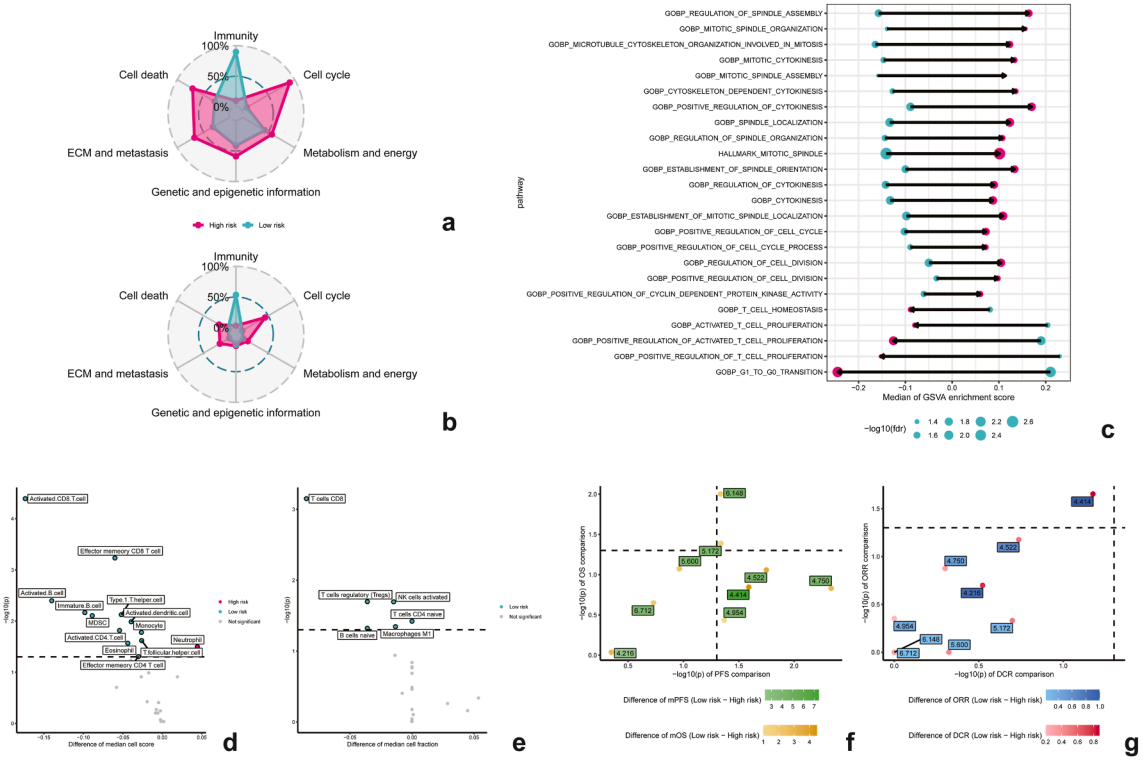


Fig. 3. Bulk level transcriptomic data identify distinct OS risk PAAD phenotypes. **(a-b)** Radar plot for GSVA results **(c)** Dumbbell plot for GSVA results **(d)** Volcano plot for ssGSEA results **(e)** Volcano plot for CIBERSORT results **(f)** Scatter plot for PFS/OS **(g)** Scatter plot for DC/OR.

GSVA score, we researched the Spearman correlation by using the model risk score as a continuous variable. All Spearman correlation results were provided in Supplementary Table-5, and the four gensets with the relative high correlation coefficient were showed in scatter plots (Fig. S4c–S4f). The risk score was negatively correlated with the GSVA score of "GOBP POSITIVE REGULATION OF ACTIVATED T-CELL PROLIFERATION" ($r = -0.464$, $p < 0.001$) and "GOBP G1 TO G0 TRANSITION" ($r = -0.546$, $p < 0.001$), and was positively correlated with the GSVA score of "HALLMARK MITOTIC SPINDLE" ($r = 0.484$, $p < 0.001$) and "GOBP REGULATION OF CELL DIVISION" ($r = 0.511$, $p < 0.001$).

3.4. TIME analysis

After comparing ssGSEA results (Supplementary Table-6), 15 from 28 immune cell types were significantly different between the high and low risk groups (Fig. 3d). In which, "Activated.CD8.T.cell" (0.522 vs. 0.695, $p < 0.001$, Fig. S5a), "Effector memory CD8 T cell" (0.594 vs. 0.654, $p < 0.001$, Fig. S5b), "Type.1.T.helper.cell" (0.507 vs. 0.559, $p = 0.007$, Fig. S5c), "Activated.CD4.T.cell" (0.419 vs. 0.474, $p = 0.015$, Fig. S5d) and "Effector memory CD4 T cell" (0.469 vs. 0.499, $p = 0.049$, Fig. S5e) showed higher score in the low risk group with statistically significant. In terms of high risk group, only "Neutrophil" (0.152 vs. 0.107, $p = 0.032$, Fig. S5f) performed higher score.

We also compared four ESTIMATE score between the high and low risk groups (Supplementary Table-7). Results showed that Stromal Score (300.66 vs. 674.05, $p = 0.146$, Fig. S5g), Immune Score (697.35 vs. 1747.89, $p < 0.001$, Fig. S5h), ESTIMATE Score (1351.04 vs. 2350.37, $p = 0.005$, Fig. S5i) had a higher median value in the low risk group. And TumorPurity (0.69 vs. 0.58, $p = 0.005$, Fig. S5j) had a higher median value in the high risk group.

The comparison result of CIBERSORT were in Supplementary Table-8, and five from 22 immune cell types were significantly different between the high and low risk groups (Fig. 3e). All the five kinds of immune cells displayed the higher fraction in the low-risk group. In the CIBERSORT algorithm, the fraction of two pairs of immune cells with reverse roles in the TIME were simulated, and the comparison result of the four cells between the high and low risk groups were displayed. The fraction of T cells CD8 (2.09% vs. 10.61%, $p < 0.001$, Fig. S5k), T cells regulatory (Tregs) (2.57% vs. 6.17%, $p = 0.020$, Fig. S5l) and Macrophages M1 (0.90% vs. 2.24%, $p = 0.045$, Fig. S5m) were higher in the low risk group, whereas Macrophages M2 (15.33% vs. 10.85%, $p = 0.692$, Fig. S5n) was higher in the high risk group.

3.5. ICIs' effect analysis

To evaluate the potential efficacy of the risk model in ICIs therapy, the correlation between IPSs and risk score was first investigated (Supplementary Table-9). The "IPS: PD-1/PD-L1 blocker", "IPS: CTLA-4 blocker" and "IPS: CTLA-4 and PD-1/PD-L1 blocker" was negatively correlated with risk score, with the Spearman correlation coefficient of −0.432 ($p = 0.007$), −0.454 ($p = 0.004$) and −0.341 ($p = 0.036$), respectively (Fig. S6a). In subgroup analysis, there was no statistical significant results in high risk group, whereas in low risk group "IPS: PD-1/PD-L1 blocker" ($r = -0.695$, $p < 0.001$), "IPS: CTLA-4 blocker" ($r = -0.518$, $p < 0.05$) and "IPS: CTLA-4 and PD-1/PD-L1 blocker" ($r = -0.660$, $p < 0.01$) were still negatively correlated with risk score (Fig. S6a).

To further explore value of the risk model in ICIs therapy, real world data from a phase II clinical study[14] were used to conduct risk assessment combined with the our risk model (Supplementary Table-10). The efficacy of the model score in predicting PFS, OS, objective response (OR) and disease control (DC) was explored. The result of univariate COX analysis showed that the model score was a risk factor for both PFS ($p = 0.029$, $HR = 3.313$, 95%*CI*: 1.133–9.690) and OS ($p = 0.042$, $HR = 2.629$, 95% *CI*: 1.037–6.666) (Fig. S6b). The result of receiver operating characteristic curve (ROC) analysis suggested that the model score had a high accuracy in predicting DC ($AUC = 0.857$, 95% *CI*: 0.548–1.000, Fig. S6c) and OR ($AUC = 1.000$, 95% *CI*: 95% *CI*, Fig. S6d) for PAAD patients accepting ICIs therapy. In order to better apply the risk model into the clinic, we further explored the best possible cut-off value for the ICIs therapy. For time-to-event prognostic items, 6.148 was the best cut-off value (Fig. 3f). In terms of response rate, 4.414 might be the best cut-off value (Fig. 3g).

3.6. Single-cell and spatial analysis revealed the immunosuppressive role of high risk score cells

A total of 16 PAAD samples were analyzed, resulting in the identification of 14,675 cells for single-cell analysis.[15] The cells were categorized into five main clusters based on curated classical markers: epithelial cells, myeloid cells, fibroblasts, endothelial cells, T/B cells (Fig. 4a). We exploited the AUCell algorithm to calculate the risk score in all cell types, revealing a subset of malignant cells having the highest risk score.

We classified malignant cells into two subtypes based on their risk scores: those with the highest risk scores (top 50%) were grouped as the high-risk score group, while those with the lowest risk scores (bottom 50%) were categorized as the low-risk score group. To investigate the disparities in biological function between these two groups, we conducted a differential expression analysis. The top five up-regulated genes in malignant cells with high risk scores were identified as *REG1A*, *PRSS1*, *REG1B*, *REG3G*, and *IGF2* (Fig. 4b).

DEGs between malignant cells with high and low risk scores were subjected to GSEA. The results indicated that genes up-regulated in malignant cells with high risk scores were significantly enriched in pathways associated with angiogenesis and DM (Fig. 4c). Furthermore, pathways related to proliferation, including the cell cycle and MYC targets, were also up-regulated in the high-risk score group, suggesting an aggressive phenotype of these tumor cells.

Conversely, genes up-regulated in malignant cells with low risk scores were enriched in pathways associated with T cell-mediated cytotoxicity and lymphocyte-mediated immunity, indicating an enhanced immune response in these low-risk malignant cells (Fig. 4c). We then utilized the spatial transcriptomics data of one PAAD sample aquired from GSE224411 to exploit the Tumor microenvironment (TME) feature of high risk score spots.[16] We first clustered 1872 spots into 12 clusters and recognized the cluster 8 as the tumor cluster based on the hematoxylin-eosin (HE) information of this sample (Fig. 4d and e). We calculated the risk score for each spots in cluster 8 and labeled the spots with top 50% risk score as the high risk score spots. We found the high risk score spots closely located with cluster 6, which was infiltrated by myeloid cells based on the high expression of myeloid markers (CD14, CD163 and CD68) (Fig. 4f). These results indicated the co-location of myeloid cells and high risk score spots might foster the local inflammation of PAAD TME.

To fully investigate the cell–cell communication related to high risk score cells, we perfomed CellChat analysis. The result showed high risk score cells had the strongest outgoing interaction strength among all cell types (Fig. 5a and b). High-risk score cells were found to initiate a diverse array of signaling pathways, including MIF, MK, PARs, GDF, and IGF. Conversely, they received signals from various pathways, such as MK, RESISTIN, TWEAK, and FGF (Fig. 5c).

Notably, we identified major ligand–receptor pairs involved in the intercellular communication between high-risk score cells and endothelial cells, including VEGFA-VEGFR1 and VEGFA-VEGFR2. This finding strongly suggests the pro-angiogenic activity of high-risk score cells within the local microenvironment. Moreover, our analysis revealed several receptor–ligand pairs between high-risk score cells and immune cells. Specifically, MDK was found to activate NCL in T cells (Fig. 5d). Additionally, signaling from high-risk score cells via MIF was observed to activate (CD74+CXCR4) and (CD74+CD44) in myeloid cells and T cells, potentially inducing an immunosuppressive effect on these

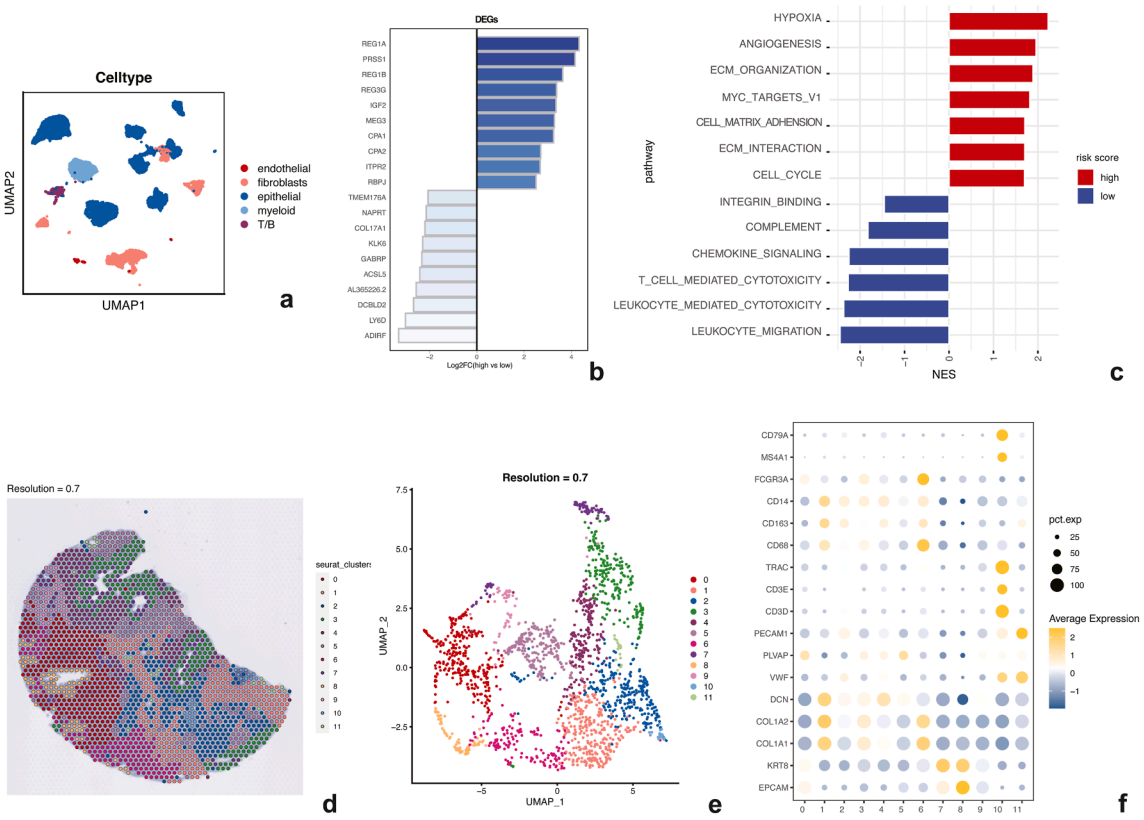


Fig. 4. Single-cell and spatial analysis revealed the phenotype of high risk score cells. **a** All cells were categorized into five main clusters based on curated classical markers: epithelial cells, myeloid cells, fibroblasts, endothelial cells, T/B cells **b** The top up-regulated and down-regulated genes in high risk score malignant cells **c** The top up-regulated and down-regulated pathways in high risk score malignant cells **d** The spatial location of clusters of one PAAD sample in spatial analysis **e** UMAP plot displayed the clusters of one PAAD sample in spatial analysis **f** The marker genes of each cluster in spatial analysis.

cell types. In the meanwhile, many immunosuppressive ligand–receptor pairs, including TNFSF12-TNFRSF12A, SPP1-CD44 and LGALS9-CD44 had been observed in the communication between myeloid cells and high risk score cells (Fig. 5d).

3.7. Inhibition of ACACA and ATG7 impairs migration, induces G1 arrest, and modulates apoptosis in a glucose-dependent manner

Among the 10 identified marker genes in PAAD patients with DM, we further investigated the roles of *ACACA* and *ATG7*, the most significantly correlated genes with prognosis in PAAD. *ACACA* encodes acetyl-CoA carboxylase 1 (ACC1), a biotin-dependent enzyme that catalyzes the carboxylation of acetyl-CoA to generate malonyl-CoA, the first and rate-limiting step in de novo fatty acid synthesis. ACC1 is critical for lipogenesis, metabolic regulation and cellular proliferation. *ACACA* activity is tightly regulated by hormones (e.g., insulin), nutrients (e.g., glucose), and energy sensors (e.g., AMPK phosphorylates and inhibits ACC1 under low-energy conditions). Dysregulation of *ACACA* is linked to metabolic disorders (e.g. obesity, DM) and cancer progression.

ATG7 is a key regulator in autophagy, functioning as an E1-like enzyme to activate ATG12 and LC3 proteins during autophagosome formation. Aberrant *ATG7*-mediated autophagy has been implicated in tumor progression, metabolic adaptation, and therapy resistance. To investigate the functional roles of *ACACA* and *ATG7*, we silenced these genes using specific siRNAs (Fig. S7a–e) in PANC-1 and MIA PaCa-2 cells cultured under 5.5, 25, and 50 mM glucose concentrations. Their effects on cell proliferation, migration, apoptosis and the cell cycle were assessed through the CCK-8 assay, flow cytometry and transwell experiments.

First, in MIA PaCa-2 cells, the inhibition of *ACACA* and *ATG7* significantly reduced migration, with *siATG7* exerting a more pronounced effect under higher glucose concentrations (Fig. 6a). In PANC-1 cells, migration was markedly reduced upon *siACACA* or *siATG7* treatment except at 5.5 mM glucose concentration (Fig. 6b). Inhibiting *ACACA* likely impairs cell migration by disrupting fatty acid synthesis, which may reduce membrane phospholipid levels and compromise membrane fluidity. Additionally, autophagy has been implicated in epithelial–mesenchymal transition (EMT) in tumor cells, a process known to enhance migratory capacity. Therefore, *ATG7* inhibition may impaire autophagy-mediated EMT. Moreover, both cell lines were more dependent on *ACACA* and *ATG7* function under high-glucose concentration, as migration capacity increased with rising glucose concentrations (Fig. S7f and S7g), further validating that PAAD is more likely to metastasize in a high-glucose environment.

Next, we examined the cell cycle using flow cytometry. An increased proportion of cells in the G1 phase was observed upon *siACACA* and *siATG7* treatment in both cell lines, accompanied by a corresponding decrease in the S phase. Notably, *siACACA* induced a more pronounced G1 phase arrest than *siATG7* (Fig. 6c and d), suggesting that ACACA-mediated fatty acid synthesis is vital to cell division, as phospholipids and fatty acids are essential for membrane formation and signal transduction. Furthermore, *ATG7* inhibition impaired the autophage process, reducing an alternative source of phospholipids and metabolic intermediates necessary for cell proliferation.

In MIA PaCa-2 cells, G1 arrest was observed with increasing glucose concentrations, regardless of the intervention group. Nevertheless, the trend was reversed in PANC-1 cells, with the proportion of cells in the G1 phase decreasing as glucose concentration increased (Fig. S7h–m). This finding suggests that elevated glucose levels may promote cell cycle progression in PANC-1 cells while inducing metabolic stress in MIA PaCa-2 cells, thus leading to cell cycle arrest. These results indicate that the PANC-1 cell line may be more dependent on glycolysis for energy production.

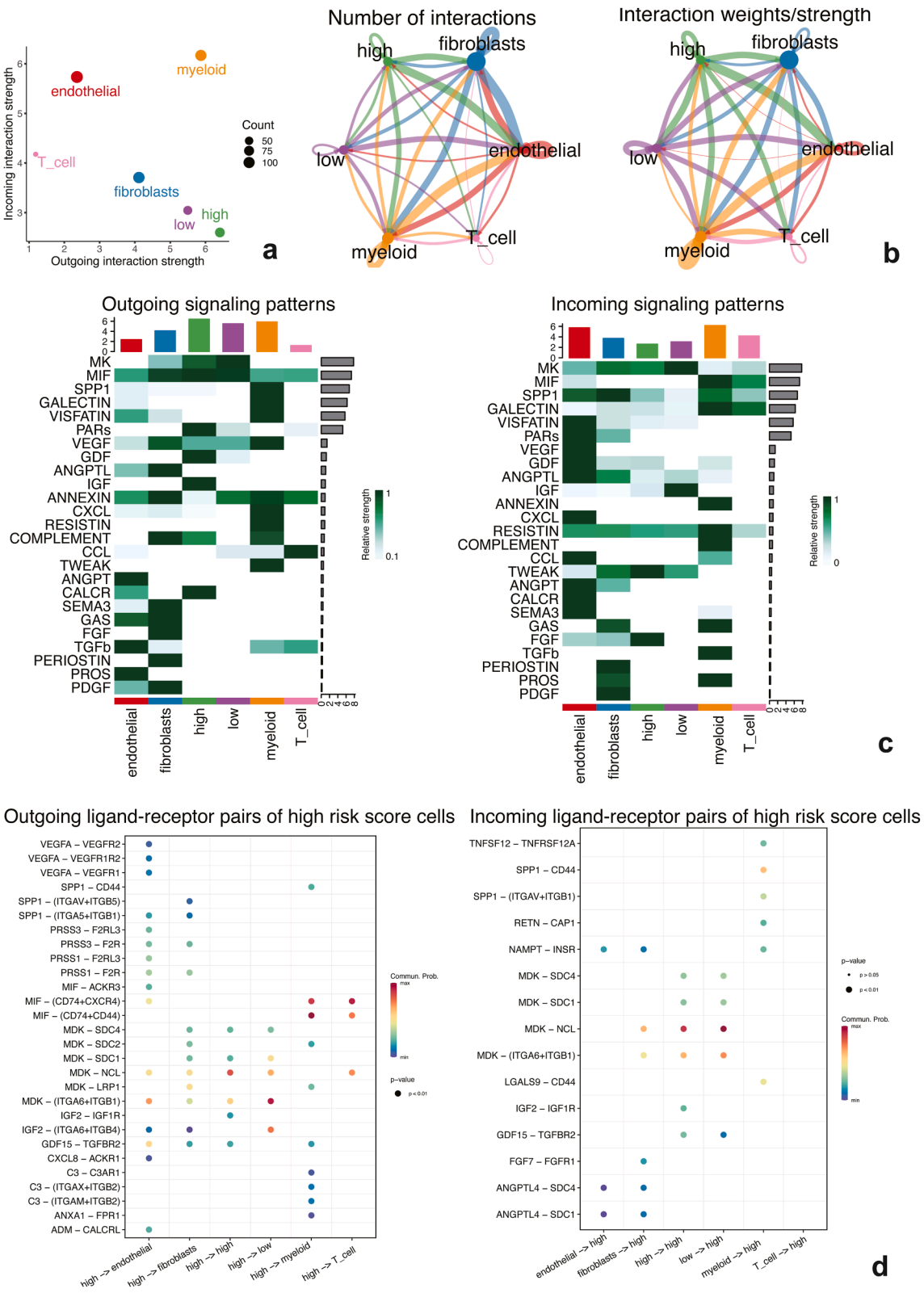


Fig. 5. High risk score cells modulated complex cell–cell communication in TME. **a** The incoming and outgoing signaling interaction strength of all cell types **b** The number of interactions and interaction weights among each cell type **c** The outgoing (left) and incoming (right) signaling patterns of all cell types **d** The ligand–receptor pairs signaled from high risk score to other cell types (left) and signaled from other cell types to high risk score (right).

After confirming the tumor-promoting roles of *ACACA* and *ATG7*, we examined apoptosis rates under the same conditions. Contrary to our expectations, *siATG7* treatment reduced apoptosis in both cell lines under high-glucose concentrations (Fig. 6e and f), which was inconsistent with the cytoprotective role of autophagy. Upon literature review, we found that *ATG7* silencing in PANC-1 cells decreased lipid peroxidation products and limited ferroptosis.[25] Meanwhile, elevated glucose levels enhanced oxidative stress and induced lipid peroxidation,

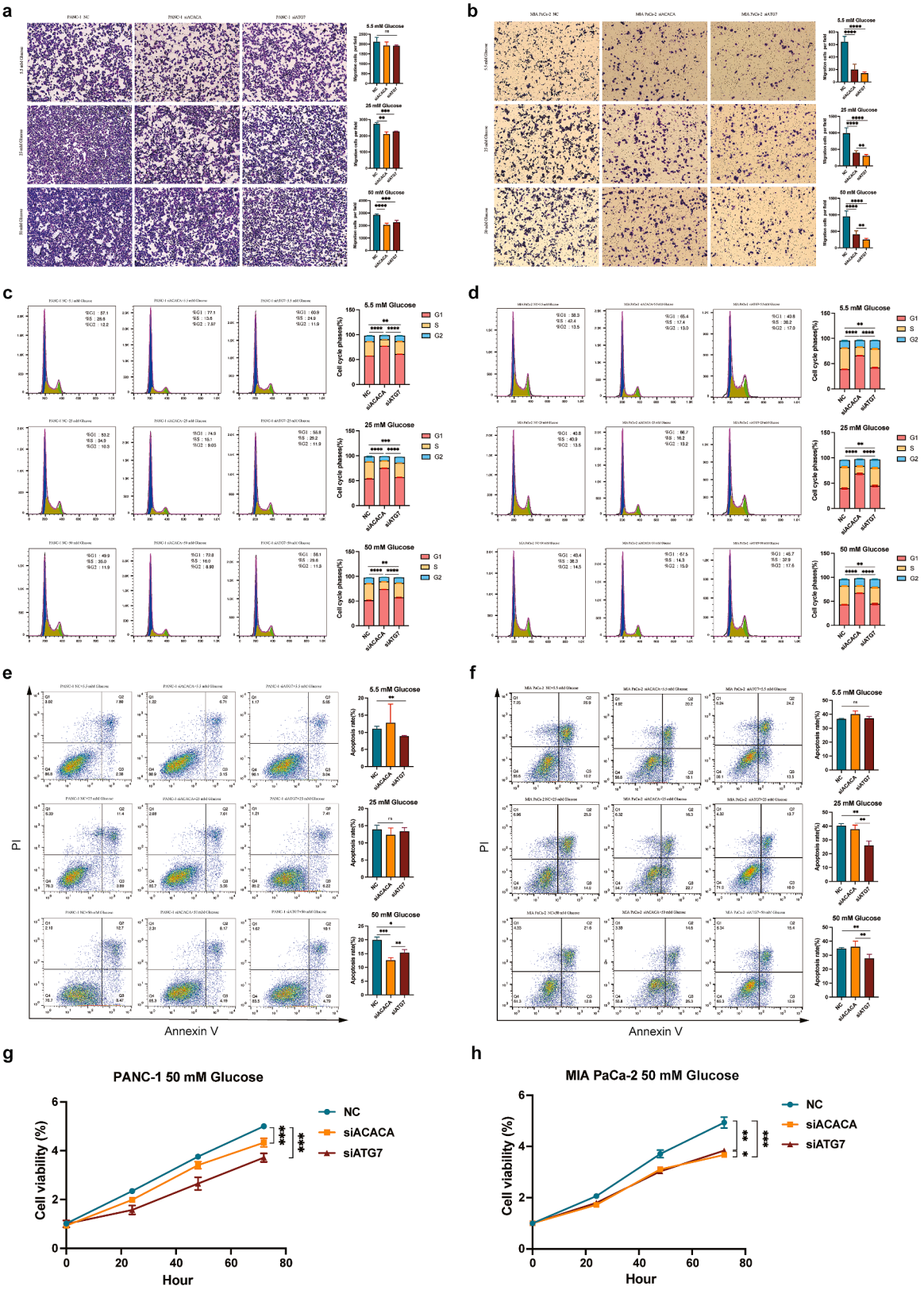


Fig. 6. Inhibition of *ACACA* and *ATG7* impairs migration, induces G1 arrest, and modulates apoptosis in a glucose-dependent manner. **(a–b)** Transwell assays showing migration capacity of PANC-1 **(a)** and MIA PaCa-2 **(b)** cells after siRNA-mediated knockdown of *ACACA* and *ATG7* under different glucose concentrations. **(c–d)** Flow cytometry analysis of the cell cycle under different glucose concentrations. Flow cytometry histograms and corresponding quantitative bar graphs showed the distribution of cells in different phases of the cell cycle in PANC-1 **(c)** and MIA PaCa-2 cells **(d)**. **(e–f)** Apoptosis analysis using Annexin V/PI staining under varying glucose concentrations. Flow cytometry dot plots and net percentages of apoptotic cells were shown in PANC-1 **(e)** and MIA PaCa-2 cells **(f)**. **(g–h)** Cell proliferation of PANC-1 **(g)** and MIA PaCa-2 **(h)** cells measured by CCK-8 assay over 72 h at 50 mM glucose.

both of which contribute to apoptosis. These findings explain the anti-apoptosis effect of *siATG7*, particularly under high-glucose concentrations. They also align with the increase in apoptosis rates as glucose concentration rose in the NC and *siATG7* groups in PANC-1 cells. However, in the *siACACA* group, apoptosis rates remained unchanged across all glucose concentrations, leading to the lowest apoptosis rate at 50 mM glucose compared to the NC and *siATG7* groups (Fig. S7n–p). It can be explained by the disruption of fatty acid synthesis, which sharply reduced the substrate availability for lipid peroxidation, thereby mitigating oxidative stress caused by glucose.

In contrast, in MIA PaCa-2 cells, the *siACACA* group showed no significant difference in apoptosis rates compared to the NC group, while apoptosis in the *siATG7* group decreased at high-glucose concentrations compared to 5.5 mM glucose (Fig. S7q-s). These results implied that the MIA PaCa-2 cell line may, on the one hand, exhibit metabolic compensation for fatty acid deficiency and, on the other hand, activate alternative survival pathways (such as upregulating antioxidant enzymes or activating the NRF2 pathway) to counteract oxidative damage induced by autophagy inhibition.

Finally, we assessed cell proliferation curves at 50 mM glucose concentration. Inhibition of both *ACACA* and *ATG7* significantly reduced cell proliferation (Fig. 6g and h), further validating their tumor-promoting effect in a high-glucose environment. These findings also verified the accuracy of the risk model.

4. Discussion

PAAD remains a significant clinical challenge, characterized by a poor prognosis. Standard treatment options have resulted in disappointing outcomes, with a 5-year OS rate below 5% and a 1-year OS rate at 24%.[26,27] Hyperglycemia and hyperinsulinemia in patients with type 2 DM (T2DM) are recognized risk factors for the development of pancreatic cancer. Conversely, pancreatic cancer cells can induce dysfunction of pancreatic β-cells through autocrine and paracrine secretion, resulting in the onset of pancreatogenic DM.[28] Epidemiological evidence supporting the increased risk of PAAD in individuals with longstanding T2DM as well as those with new-onset pancreatogenic DM has been extensively reviewed in previous studies. Furthermore, the proposed mechanisms underlying this increased risk have been thoroughly investigated.[2,29,30] However, information regarding the clinical profile of PAAD patients with DM is limited.

Unlike most existing models that primarily predict pancreatic cancer risk in DM populations, our novel 10-gene model was specifically designed to stratify survival outcomes in patients diagnosed with both PAAD and DM. By leveraging newly identified DM-associated marker genes, this model not only predicts OS but also offers potential clinical utility: low-risk patients may be suitable for ICIs, whereas high-risk patients could benefit from alternative approaches such as anti-angiogenic therapy. These genes further represent promising therapeutic targets, providing a new avenue for personalized treatment strategies in this comorbid population. ACACA - Catalyzes the rate-limiting reaction in the biogenesis of long-chain fatty acids, increasing fatty acid synthesis via the fatty acid metabolism pathway. The detection of *ACACA* could increases fatty acid synthesis and lipid accumulation, its dysregulation provides a direct molecular link between DM states and altered lipid metabolism fueling tumor growth, as evidenced in cancers like hepatocellular carcinoma and prostate cancer.[31,32] *ATG7*-a core autophagy-related gene, plays a crucial role in protecting cells from cytotoxicity by degrading toxic protein aggregates, pathogens, and damaged organelles. Additionally, it maintains homeostasis by recycling essential metabolites.[33] *ATG7* has been identified as being with neurodevelopmental disorder.[34] Traditionally, the loss of mammalian *ATG7* is considered to render cells and tissues "autophagy deficient".[35–37] *DEFB123* is a member of the beta-defensin family, annotated as being involved in immune processes, particularly in the innate immune response.[38,39] *FSTL3* has been shown to regulate multiple biological processes, including cell differentiation and metastasis,[40–42] making it a relevant factor for prognostic stratification in cancer. *RASSF1* is a putative tumor suppressor gene whose inactivation is implicated in the development of many human cancers. It regulates tumor growth by inhibiting the RAS pathway.[43–46] Additionally, *RASSF1* is one of the most frequently reported methylation-inactivated tumor suppressor genes in primary PAAD.[47] Its selection underscores the importance of tumor suppressor loss in PAAD pathogenesis, potentially exacerbated in a DM context. *RBPJ* has been reported to be involved in RBPJ-dependent tumor-associated macrophages (TAMs) that promote tumor immune tolerance, in part by modulating the $CD8^+$ T cell response.[48,49] This links the gene directly to the modulation of the TIME. *SLC35F2* might be highly expressed in aggressive and invasive tumor cells[50] and functions as a solute carrier protein for YM155 uptake, which leads to DNA damage,[51] implicating it in tumor cell proliferation and stress adaptation. *SLC37A1* has been proposed to transport glycerol-3-phosphate and has been shown to exert a critical regulatory role in tumor cell proliferation.[52,53] *ZC3H12D*, a well-characterized negative regulator, has been implicated in immune modulation and contributes significantly to tumor immune infiltration.[54] Emerging mechanistic evidence demonstrates that *ZC3H12D* serves as a novel negative feedback regulator of Toll-like receptor signaling pathways, directly suppressing macrophage activation and thus may play a role in host immunity and inflammatory diseases.[55] This role in modulating inflammatory signaling and immune cell function within the TME aligns with the chronic inflammatory state associated with DM. Integrated multi-omics analyses demonstrate that the identified marker genes mechanistically bridge immune response pathways and apoptotic cascades, establishing a functional link between tumor immunosurveillance and programmed cell death. Together, these genes—spanning metabolic/autophagy regulators and immune/TME-associated factors—provide mechanistic grounding for our DM-based model, which captures both the proliferative/angiogenic and immunosuppressive programs heightened in PAAD under hyperglycemic conditions.

Through in vitro functional studies, we validated the oncogenic roles of *ACACA* and *ATG7* in PAAD cells, demonstrating their impact on migration, cell cycle progression, apoptosis, and proliferation, particularly under high-glucose conditions. Their knockdown significantly impaired migration, induced G1 arrest (with *siACACA* having a stronger effect), and suppressed tumor growth, highlighting their roles in cell motility, division, and proliferation. Notably, *siATG7* unexpectedly reduced apoptosis in a high-glucose environment, likely by limiting lipid peroxidation and ferroptosis, while *siACACA* did not significantly induce apoptosis, possibly due to decreased oxidative stress from inhibition of fatty acid synthesis.

These findings reinforce *ACACA*'s role in fatty acid synthesis-driven tumor progression and *ATG7*'s function in autophagy-mediated metabolic adaptation. Given the interplay between DM, lipid metabolism, and PAAD progression, targeting these pathways could provide novel therapeutic opportunities.

In recent years, there has been a growing recognition of the significance of immunotherapy in cancer treatment.[56–58] PD-L1 serves as the primary ligand for PD-1 and is often overexpressed and detected in various solid human cancers, including PAAD.[59] However, PAAD has a highly immunosuppressive desmoplastic TIME where ICIs therapy has been exceptionally ineffective.[22,60,61] As recent study shows that systemic low-grade inflammation is a feature of T2DM which may cause the dysregulation of immunometabolism.[62,63] According to our analysis, the PAAD patients with DM were more active in immune pathway than those without DM (Fig. S1b and S1c), and the low risk group PAAD patients with DM meant an immune phenotype. Our model not only had a high value in predicting the efficacy of ICIs from IPSs (Fig. S6a), but also in predicting PFS, OS, OR and DC from the real world data (Fig. S6b–S6d). Crucially, our model transcends prognostic stratification by offering actionable insights for immunotherapy selection in the challenging context of DM-associated PAAD.

The risk model has also been validated at the single-cell transcriptomic level, with the low-risk group exhibiting an immune-active phenotype. Additionally, single-cell transcriptomic data results further indicated that vascular-related pathways were more active in the high-risk group, suggesting a potential suitability for anti-angiogenic therapy, which may provide a basis for personalized treatment of PAAD patients with DM.

Building upon our findings that PAAD patients with DM exhibit a more immunologically active TME and potentially greater responsiveness to ICIs therapy compared to non-DM patients, our model further enables refined stratification within the DM cohort itself. Specifically, the high-risk subgroup is characterized by a poor prognosis, a relatively "cold" TIME with lower immune cell infiltration, and heightened angiogenic pathway activity; thus, anti-angiogenic therapy is recommended. Conversely, the low-risk subgroup displays a "hot" TIME phenotype and appears more suitable for first-line ICIs therapy.

In summary, the 10-gene DM-based prognostic model not only reliably stratifies survival risk in PAAD patients with comorbid DM but also provides directly actionable guidance for personalized therapy selection. By distinguishing patients likely to benefit from ICIs therapy from those who may require alternative strategies such as anti-angiogenic treatment, this model holds significant potential to inform clinical decision-making and improve outcomes in this challenging population.

CRediT authorship contribution statement

Le Tang: Writing – review & editing, Writing – original draft, Formal analysis, Data curation, Conceptualization. **Mengwei Yang:** Writing – review & editing, Writing – original draft, Visualization, Software, Methodology, Formal analysis. **Tongji Xie:** Writing – review & editing, Writing – original draft, Visualization, Validation, Software, Methodology, Formal analysis. **Guangyu Fan:** Writing – original draft, Visualization, Formal analysis, Data curation. **Haohua Zhu:** Methodology, Data curation. **Jiari Yao:** Data curation. **Xiaohong Han:** Supervision, Investigation, Conceptualization. **Yuankai Shi:** Supervision, Investigation, Funding acquisition, Conceptualization.

Advantages and limitations of this study

We focused on the PAAD patients associated with DM, and the differences between DM and non-DM were systematically studied from transcriptomics. A robust prognostic risk model was constructed using LASSO-COX method, which provided a threshold for clinical practice, and two different phenotypes were identified according to the risk model score. Furthermore, through ICIs therapy data and single-cell data, an individualized treatment system was formed. This study still faced certain limitations. Primarily, the real-world study was constrained by its sample size. Additionally, the ICIs therapy data and single-cell data were obtained from the PAAD population without specific information on DM. Moreover, our multi-omics and ICIs therapy analyses relied primarily on retrospectively collected public datasets (TCGA and GEO), which may introduce selection bias and technical heterogeneity that cannot be completely eliminated. Therefore, further investigations involving larger sample sizes are warranted to draw more reliable conclusions. Such studies would provide more precise insights into identifying beneficiaries within the PAAD patients with DM during clinical practice.

Ethics approval and consent to participate

This study utilized only (1) pre-existing, de-identified data from public databases and (2) commercially available cell lines. Therefore, ethical approval and the need for informed consent were waived for this work. The research was conducted in accordance with the principles outlined in the Declaration of Helsinki.

Consent for publication

Not applicable.

Data availability

The datasets used and analyzed during the current study are available from the corresponding author on reasonable request.

Declaration of competing interest

The authors declare that they have no known competing financial interests or personal relationships that could have appeared to influence the work reported in this paper.

Acknowledgements

This work was supported by the National Science and Technology Major Project for Key New Drug Development (2017ZX09304015). The authors have no other relevant affiliations or financial involvement with any organization or entity with a financial interest in or financial conflict with the subject matter or materials discussed in the manuscript apart from those disclosed.

Appendix A. Supplementary data

Supplementary data to this article can be found online at https://doi.org/10.1016/j.ipha.2025.12.004.

References

1. Siegel RL, Miller KD, Wagle NS, Jemal A. Cancer statistics, 2023. *CA Cancer J Clin*. 2023;73(1):17–48.
2. Andersen DK, Korc M, Petersen GM, et al. Diabetes, pancreatogenic diabetes, and pancreatic cancer. *Diabetes*. 2017;66(5):1103–1110.
3. Badowska-Kozakiewicz A, Fudalej M, Kwaśniewska D, et al. Diabetes mellitus and pancreatic ductal adenocarcinoma-prevalence, clinicopathological variables, and clinical outcomes. *Cancers*. 2022;14(12):2840.
4. Yang J, Wen C, Guo H, Chai Y, Sun G, Cheng H. Targeting early diagnosis and treatment of pancreatic cancer among the diabetic population: a comprehensive review of biomarker screening strategies. *Diabetol Metab Syndr*. 2025;17(1):176.
5. Liao WC, Tu YK, Wu MS, Lin JT, Wang HP, Chien KL. Blood glucose concentration and risk of pancreatic cancer: systematic review and dose-response meta-analysis. *BMJ*. 2015;350:g7371.
6. Aggarwal G, Kamada P, Chari ST. Prevalence of diabetes mellitus in pancreatic cancer compared to common cancers. *Pancreas*. 2013;42(2):198–201.
7. Paternoster S, Falasca M. The intricate relationship between diabetes, obesity and pancreatic cancer. *Biochim Biophys Acta Rev Cancer*. 2020;1873(1):188326.
8. Eibl G, Cruz-Monserrate Z, Korc M, et al. Diabetes mellitus and obesity as risk factors for pancreatic cancer. *J Acad Nutr Diet*. 2018;118(4):555–567.
9. Ioannou LJ, Maharaj AD, Zalcberg JR, et al. Prognostic models to predict survival in patients with pancreatic cancer: a systematic review. *HPB*. 2022;24(8):1201–1216.
10. Cheng Y, Wang K, Geng L, et al. Identification of candidate diagnostic and prognostic biomarkers for pancreatic carcinoma. *EBioMedicine*. 2019;40:382–393.
11. Zhou Q, Chen X, Chen Q, Liu H, Hao L. A four autophagy-related gene-based prognostic signature for pancreatic cancer. *Crit Rev Eukaryot Gene Expr*. 2021;31(4):89–100.
12. Hou Z, Pan Y, Fei Q, et al. Prognostic significance and therapeutic potential of the immune checkpoint VISTA in pancreatic cancer. *J Cancer Res Clin Oncol*. 2021;147(2):517–531.
13. Kirby MK, Ramaker RC, Gertz J, et al. RNA sequencing of pancreatic adenocarcinoma tumors yields novel expression patterns associated with long-term survival and reveals a role for ANGPTL4. *Mol Oncol*. 2016;10(8):1169–1182.
14. Parikh AR, Szabolcs A, Allen JN, et al. Radiation therapy enhances immunotherapy response in microsatellite stable colorectal and pancreatic adenocarcinoma in a phase II trial. *Nat Cancer*. 2021;2(11):1124–1135.
15. Lin W, Noel P, Borazanci EH, et al. Single-cell transcriptome analysis of tumor and stromal compartments of pancreatic ductal adenocarcinoma primary tumors and metastatic lesions. *Genome Med*. 2020;12(1):80.
16. Deshpande A, Loth M, Sidiropoulos DN, et al. Uncovering the spatial landscape of molecular interactions within the tumor microenvironment through latent spaces. *Cell Syst*. 2023;14(4):285–301.e4.
17. Hänzelmann S, Castelo R, Guinney J. GSVA: gene set variation analysis for microarray and RNA-seq data. *BMC Bioinf*. 2013;14:7.

18. Subramanian A, Tamayo P, Mootha VK, et al. Gene set enrichment analysis: a knowledge-based approach for interpreting genome-wide expression profiles. *Proc Natl Acad Sci U S A*. 2005;102(43):15545–15550.
19. Szklarczyk D, Gable AL, Nastou KC, et al. The STRING database in 2021: customizable protein-protein networks, and functional characterization of user-uploaded gene/measurement sets. *Nucleic Acids Res*. 2021;49(D1):D605–D612.
20. Inferring tumour purity and stromal and immune cell admixture from expression data - PubMed. Accessed May 14, 2023.
21. Newman AM, Liu CL, Green MR, et al. Robust enumeration of cell subsets from tissue expression profiles. *Nat Methods*. 2015;12(5):453–457.
22. Charoentong P, Finotello F, Angelova M, et al. Pan-cancer immunogenomic analyses reveal genotype-immunophenotype relationships and predictors of response to checkpoint blockade. *Cell Rep*. 2017;18(1):248–262.
23. Charoentong P, Finotello F, Angelova M, et al. Pan-cancer immunogenomic analyses reveal genotype-immunophenotype relationships and predictors of response to checkpoint blockade. *Cell Rep*. 2017;18(1):248–262.
24. Givechian KB, Wnuk K, Garner C, et al. Identification of an immune gene expression signature associated with favorable clinical features in Treg-enriched patient tumor samples. *NPJ Genomic Med*. 2018;3:14.
25. Hou W, Xie Y, Song X, et al. Autophagy promotes ferroptosis by degradation of ferritin. *Autophagy*. 2016;12(8):1425–1428.
26. Chen W, Zheng R, Baade PD, et al. Cancer statistics in China, 2015. *CA Cancer J Clin*. 2016;66(2):115–132.
27. Reyes-Gibby CC, Chan W, Abbruzzese JL, et al. Patterns of self-reported symptoms in pancreatic cancer patients receiving chemoradiation. *J Pain Symptom Manage*. 2007;34(3):244–252.
28. Pannala R, Leirness JB, Bamlet WR, Basu A, Petersen GM, Chari ST. Prevalence and clinical profile of pancreatic cancer-associated diabetes mellitus. *Gastroenterology*. 2008;134(4):981–987.
29. Hart PA, Bellin MD, Andersen DK, et al. Type 3c (pancreatogenic) diabetes mellitus secondary to chronic pancreatitis and pancreatic cancer. *Lancet Gastroenterol Hepatol*. 2016;1(3):226–237.
30. Sah RP, Nagpal SJS, Mukhopadhyay D, Chari ST. New insights into pancreatic cancer-induced paraneoplastic diabetes. *Nat Rev Gastroenterol Hepatol*. 2013;10(7):423–433.
31. Zhang H, Liu S, Cai Z, et al. Down-regulation of ACACA suppresses the malignant progression of Prostate Cancer through inhibiting mitochondrial potential. *J Cancer*. 2021;12(1):232–243.
32. Peng JY, Cai DK, Zeng RL, et al. Upregulation of Superenhancer-Driven LncRNA FASRL by USF1 Promotes De Novo Fatty Acid Biosynthesis to Exacerbate Hepatocellular Carcinoma. *Adv Sci Weinh Baden-Wurtt Ger*. 2022;10(1):e2204711.
33. Galluzzi L, Baehrecke EH, Ballabio A, et al. Molecular definitions of autophagy and related processes. *EMBO J*. 2017;36(13):1811–1836.
34. Collier JJ, Guissart C, Oláhová M, et al. Developmental consequences of defective ATG7-Mediated autophagy in humans. *N Engl J Med*. 2021;384(25):2406–2417.
35. Komatsu M, Waguri S, Ueno T, et al. Impairment of starvation-induced and constitutive autophagy in Atg7-deficient mice. *J Cell Biol*. 2005;169(3):425–434.
36. Takamura A, Komatsu M, Hara T, et al. Autophagy-deficient mice develop multiple liver tumors. *Genes Dev*. 2011;25(8):795–800.
37. Xiong J. Atg7 in development and disease: Panacea or Pandora's Box? *Protein Cell*. 2015;6(10):722–734.
38. Chen Y, Tibbs-Cortes LE, Ashley C, et al. The genetic basis of natural antibody titers of young healthy pigs and relationships with disease resilience. *BMC Genom*. 2020;21(1):648.
39. Motzkus D, Schulz-Maronde S, Heitland A, et al. The novel beta-defensin DEFB123 prevents lipopolysaccharide-mediated effects in vitro and *in vivo*. *FASEB J Off Publ Fed Am Soc Exp Biol*. 2006;20(10):1701–1702.
40. Hayette S, Gadoux M, Martel S, et al. FLRG (follistatin-related gene), a new target of chromosomal rearrangement in malignant blood disorders. *Oncogene*. 1998;16(22):2949–2954.
41. Sidis Y, Tortoriello DV, Holmes WE, Pan Y, Keutmann HT, Schneyer AL. Follistatin-related protein and follistatin differentially neutralize endogenous vs. exogenous activin. *Endocrinology*. 2002;143(5):1613–1624.
42. Sidis Y, Schneyer AL, Keutmann HT. Heparin and activin-binding determinants in follistatin and FSTL3. *Endocrinology*. 2005;146(1):130–136.
43. Dammann R, Li C, Yoon JH, Chin PL, Bates S, Pfeifer GP. Epigenetic inactivation of a RAS association domain family protein from the lung tumour suppressor locus 3p21.3. *Nat Genet*. 2000;25(3):315–319.
44. Rodriguez-Viciana P, Sabatier C, McCormick F. Signaling specificity by Ras family GTPases is determined by the full spectrum of effectors they regulate. *Mol Cell Biol*. 2004;24(11):4943–4954.
45. Shivakumar L, Minna J, Sakamaki T, Pestell R, White MA. The RASSF1A tumor suppressor blocks cell cycle progression and inhibits cyclin D1 accumulation. *Mol Cell Biol*. 2002;22(12):4309–4318.
46. Donninger H, Vos MD, Clark GJ. The RASSF1A tumor suppressor. *J Cell Sci*. 2007;120(Pt 18):3163–3172.
47. Amato E, Barbi S, Fassan M, et al. RASSF1 tumor suppressor gene in pancreatic ductal adenocarcinoma: correlation of expression, chromosomal status and epigenetic changes. *BMC Cancer*. 2016;16:11.
48. Franklin RA, Liao W, Sarkar A, et al. The cellular and molecular origin of tumor-associated macrophages. *Science*. 2014;344(6186):921–925.
49. Alsina-Sanchis E, Mülfarth R, Moll I, et al. Endothelial RBPJ is essential for the education of tumor-associated macrophages. *Cancer Res*. 2022;82(23):4414–4428.
50. Kotolloshi R, Hölzer M, Gajda M, Grimm MO, Steinbach D. SLC35F2, a transporter sporadically mutated in the untranslated Region, promotes growth, migration, and invasion of bladder cancer cells. *Cells*. 2021;10(1):80.
51. Winter GE, Radic B, Mayor-Ruiz C, et al. The solute carrier SLC35F2 enables YM155-mediated DNA damage toxicity. *Nat Chem Biol*. 2014;10(9):768–773.
52. Cappello AR, Curcio R, Lappano R, Maggiolini M, Dolce V. The physiopathological role of the exchangers belonging to the SLC37 family. *Front Chem*. 2018;6:122.
53. Iacopetta D, Lappano R, Cappello AR, et al. SLC37A1 gene expression is up-regulated by epidermal growth factor in breast cancer cells. *Breast Cancer Res Treat*. 2010;122(3):755–764.
54. Yang B, Ji LL, Xu HL, et al. Zc3h12d, a novel of hypomethylated and immune-related for prognostic marker of lung adenocarcinoma. *J Inflamm Res*. 2021;14:2389–2401.
55. Huang S, Qi D, Liang J, et al. The putative tumor suppressor Zc3h12d modulates toll-like receptor signaling in macrophages. *Cell Signal*. 2012;24(2):569–576.
56. Yousefi H, Yuan J, Keshavarz-Fathi M, Murphy JF, Rezaei N. Immunotherapy of cancers comes of age. *Expert Rev Clin Immunol*. 2017;13(10):1001–1015.
57. Riley RS, June CH, Langer R, Mitchell MJ. Delivery technologies for cancer immunotherapy. *Nat Rev Drug Discov*. 2019;18(3):175–196.
58. Brower V. Checkpoint blockade immunotherapy for cancer comes of age. *J Natl Cancer Inst*. 2015;107(3). djv069.
59. Patel SP, Kurzrock R. PD-L1 expression as a predictive biomarker in cancer immunotherapy. *Mol Cancer Ther*. 2015;14(4):847–856.
60. Schizas D, Charalampakis N, Kole C, et al. Immunotherapy for pancreatic cancer: a 2020 update. *Cancer Treat Rev*. 2020;86:102016.
61. Bear AS, Vonderheide RH, O'Hara MH. Challenges and opportunities for pancreatic cancer immunotherapy. *Cancer Cell*. 2020;38(6):788–802.
62. Donath MY, Dinarello CA, Mandrup-Poulsen T. Targeting innate immune mediators in type 1 and type 2 diabetes. *Nat Rev Immunol*. 2019;19(12):734–746.
63. Ruze R, Liu T, Zou X, et al. Obesity and type 2 diabetes mellitus: connections in epidemiology, pathogenesis, and treatments. *Front Endocrinol*. 2023;14:1161521.